Pharm Res (2015) 32:1704–1713
DOI 10.1007/s11095-014-1568-z

RESEARCH PAPER

Fractional Thermolysis by Bipolar Radiofrequency Facilitates Cutaneous Delivery of Peptide and siRNA with Minor Loss of Barrier Function

Woan-Ruoh Lee • Shing-Chuan Shen • Chi-Kuang Sun • Ibrahim A. Aljuffali • Shih-Yun Suen • Yin-Ku Lin • Jhi-Joung Wang • Jia-You Fang

Received: 29 May 2014 / Accepted: 29 October 2014 / Published online: 13 November 2014

ABSTRACT

Purpose In this study, we aimed to illustrate the utility of fractional radiofrequency (RF) that generated microchannels in the skin, allowing delivery of peptide and siRNA via the skin. The mechanisms involved in the correlation between macromolecule permeation and skin structure were also elucidated.

Methods The morphology of the skin was examined by transmission electron microscopy (TEM), higher harmonic generation microscopy (HGM), and physiological factors. *In vivo* skin distribution of macromolecules was assessed by fluorescence and confocal microscopies.

Results RF thermolysis selectively created an array of micropores deep into the epidermis without significant removal of the stratum corneum (SC). With energy of 30 mJ, a pore depth of 35 μm was achieved. The bipolar RF resulted in a 3-fold increase of transepidermal water loss (TEWL) compared with intact skin. The respective skin accumulation and flux of the peptide with a molecular weight (MW) of 2335 Da was 3- and 23-fold greater for the RF-treated group than for the non-treatment group. RF enhanced skin accumulation of siRNAs with MW of 10 and 15 kDa by 6.2- and 2.6-fold, respectively. Cutaneous penetration of the macromolecules with an MW of at least 40 kDa could be accomplished by RF. Confocal microscopy imaging revealed that RF could effectively deliver the peptide up to at least a 74-μm depth. The penetration depth of siRNA by RF irradiation was about 50 μm.

Conclusions The novel RF device efficiently delivered macromolecules into the skin while reserving SC layers to support some barrier functions. In this work, for the first time the assistance of fractional RF on peptide and siRNA transport was demonstrated.

KEY WORDS fractional ablation · peptide · radiofrequency · siRNA · skin permeation

W.-R. Lee • S.-C. Shen • S.-Y. Suen
Graduate Institute of Medical Sciences, Taipei Medical University
Taipei, Taiwan

W.-R. Lee
Department of Dermatology, Taipei Medical University
Shuang Ho Hospital, New Taipei City, Taiwan

C.-K. Sun
Graduate Institute of Photonics and Optoelectronics and Department of Electrical Engineering, National Taiwan University, Taipei, Taiwan

C.-K. Sun
Research Center for Applied Sciences and Institute of Physics
Academia Sinica, Taipei, Taiwan

I. A. Aljuffali
Department of Pharmaceutics, College of Pharmacy
King Saud University, Riyadh, Saudi Arabia

Y.-K. Lin
Department of Traditional Chinese Medicine
Chang Gung Memorial Hospital, Keelung, Taiwan

Y.-K. Lin
School of Traditional Chinese Medicine, Chang Gung University
Taoyuan, Taiwan

J.-J. Wang (✉)
Department of Medical Research, Chi-Mei Medical Center
901 Chung-Hwa Road, Yungkang Tainan, Taiwan
e-mail: 400002@mail.chimei.org.tw

J.-Y. Fang (✉)
Pharmaceutics Laboratory, Graduate Institute of Natural Products
Chang Gung University, Wen-Hwa 1st Road, Kweishan Taoyuan, Taiwan
e-mail: fajy@mail.cgu.edu.tw

J.-Y. Fang
Chinese Herbal Medicine Research Team, Healthy Aging Research Center, Chang Gung University, Kweishan Taoyuan, Taiwan

J.-Y. Fang
Research Center for Industry of Human Ecology, Chang Gung University of Science and Technology, Kweishan Taoyuan, Taiwan

INTRODUCTION

Recent advances in genetic engineering and biotechnology have encouraged development of macromolecules as drugs in the treatment of various disorders. Macromolecules such as peptides and small interfering RNA (siRNA) are currently applied for topical therapy to treat dermatological diseases (1). Some peptides reveal potential abilities for management of aging, skin infection, psoriasis, and dermatitis (2). Polypeptides are also approved for cutaneous vaccination (3). siRNA-mediated RNA interference is a kind of gene therapy that can treat skin disorders such as psoriasis, eczema, skin cancers, and genetic illness (4). Although hypodermal injection provides an efficient method for macromolecular delivery, patient compliance is always low due to the associated pain and infection risk. Topical administration offers an attractive method of delivering therapeutic macromolecules for treating skin diseases. However, the skin permeation of large permeants is highly restricted by the barrier function of the stratum corneum (SC) and the tight junction in the epidermis. A successful topical delivery of macromolecules can be achieved by skin ablation, including tape-stripping, microdermabrasion, and laser treatment. Recently, a new concept of fractional ablation has been elicited. Fractional resurfacing ablates micron-scale columns arranged in an array over a fraction of the skin surface (5). Minimal pain and quick healing are expected because of the limited area of tissue ablation (6).

The concept of fractional ablation is applied in the forms of lasers, microneedles, and radiofrequency (RF). RF is one of the innovative techniques in dermatology for skin rejuvenation. This approach produces electrical currents via an array of microelectrodes that generates heat due to resistance by the skin tissues (7). Micropores are thus created against the skin surface. Because of this characteristic, fractional RF may be feasible for assisting topical macromolecule delivery. Although the fractional modalities like lasers and microneedles are largely studies for skin-penetration enhancement (8, 9), the investigations related to RF are very few. The mechanisms of RF-assisted skin delivery are also not fully elucidated. The main objective of this work was to assess the role of a novel RF device (eMatrix®) on the topical delivery of peptide and siRNA. The RF applicator is designed to transfer bipolar RF energy on the skin in a fractional manner. The array of heating can selectively target specific tissues such as the epidermis or dermis.

Porcine skin was employed as the model permeation barrier in this study. The histology of RF-treated skin was examined by light microscopy and transmission electron microscopy (TEM). In order to further explore the mechanisms, higher harmonic generation microscopy (HGM) was utilized to analyze changes in skin structure by fractional thermolysis. Both *in vitro* and *in vivo* permeation experiments were performed to test percutaneous absorption of macromolecules assisted by RF.

MATERIALS AND METHODS

Materials

Fluorescein peptide of the form fluorescein-NH_2-Pro-Arg-Leu-Leu-Tyr-Ser-Trp-His-Arg-Ser-His-Arg-Ser-His-COOH with a molecular weight (MW) of 2335 Da was supplied by Tools Biotechnology (New Taipei City, Taiwan). Synthetic siRNAs containing fluorescein were provided by Sigma-Aldrich (St. Louis, MO, USA). The sequences of siRNAs were 5′-[fluorescein] UGCUGACUCCAAAG-3′ and 3′-ACGA CUGAGGUUUC-5′ (siRNA10, MW = 10632 Da), and 5′-[fluorescein] GCACAAGUGACUAGUCCUAUU-3′ and 3′-CGUGUUCACUGAUCAGGAUAA-5′ (siRNA 15, MW = 15111 Da). Fluorescein isothiocyanate (FITC)-dextrans of FD10 (MW = 10 kDa), FD20 (MW = 20 kDa), and FD40 (MW = 40 kDa) were also purchased from Sigma-Aldrich.

Animals

Pathogen-free, 1-week-old pigs were obtained from Animal Technology Institute Taiwan (Miaoli, Taiwan). The experimental protocol was reviewed and approved by the Institutional Animal Care and Use Committee of Chang Gung University. All animals were housed and handled based on institutional guidelines.

Bipolar Radiofrequency (RF) Assembly

The bipolar system consisted of an RF unit that generated a pulse of electromagnetic energy in a radio wave (eMatrix®, Syneron, Irvine, CA, USA). A handheld piece was used to deliver a 1 MHz current onto the skin surface. The dimension of the piece was 12×12 mm^2. This dimension had 64 pins of microelectrodes. The diameter of the pins was 200 μm. These electrodes were triggered to create micropores on the dorsal skin at 20 or 30 mJ per pin. The porcine skin received 6 passes at different angles by the operator in a dispersive mode without overlapping the micropores. The total coverage percentage of the thermolysis zone in the treated area was 4.8%.

In vivo Skin Physiology

Immediately after RF irradiation, the porcine skin was examined for physiological parameters, including transepidermal water loss (TEWL), skin surface pH, and erythema (a*). A Tewameter® (TM300, Courage and Khazaka, Köln, Germany) was employed for measuring TEWL (g/m^2/h).

The pH was determined by Skin-pH-Meter® PH905 (Courage and Khazaka). A spectrocolorimeter (CD100, Yokogawa, Tokyo, Japan) was used to quantify skin erythema.

Macroscopic Observation

The macroscopic imaging of porcine skin treated with or without RF was observed by a handheld digital microscope (Mini Scope-V, M&T Optics, Taipei, Taiwan). A magnification of 200x was used for imaging capture.

Hematoxylin and Eosin (H&E staining)

The skin was excised from the pigs after sacrifice. The skin species were immersed in a 10% buffered formaldehyde using ethanol, embedded in paraffin wax, and sliced at a thickness of 3 μm. The samples were stained by H&E and imaged under light microscopy (IX81, Olympus, Tokyo, Japan).

Transmission Electron Microscopy (TEM)

The skin was cut into cubes and fixed at 4°C in 2% paraformaldehyde and 2.5% glutaldehyde in 0.2 M cacodylate buffer overnight. The detailed process was shown in the previous study (10). The specimens were embedded in an epon-epoxy and sectioned. The samples were stained with uranyl acetate and lead citrate for TEM visualization (H600, Hitachi, Tokyo, Japan).

Higher Harmonic Generation Microscopy (HGM)

The system of HGM was adapted from a commercial confocal scanning system (FV300, Olympus) combined with an inverted microscope (IX71, Olympus) as described previously (11). A 1230-nm femtosecond Cr:forsterite laser was utilized for excitation. The harmonic signals were detected by photomultiplier tubes of the third harmonic generation (THG) and second harmonic generation (SHG). The epidermis was mapped by THG signal with a purple color. The dermis was mapped by SHG signal with a pseudo-colored green. A submicron and 1 μm resolution in lateral and axial directions was achieved with a penetration depth of >300 μm. The depth of imaging was adjusted by moving the objective in z direction.

In vitro Percutaneous Absorption

This experiment was conducted with Franz diffusion cell. The excised skin was treated by RF. The skin was then mounted between the donor and receptor compartments with SC facing upward into the donor. The receptor contained citrate-phosphate buffer (pH 7.4) with a volume of 5.5 ml. The donor was loaded with peptide (150 μM), siRNA (2 μM), or FD (150 μM) in double-distilled water (0.5 ml). The effective diffusion region for permeants was 0.785 cm^2. The temperature and stirring rate of the stirrer were kept at 37°C and 600 rpm, respectively. At determined intervals, a 300-μl aliquot was withdrawn from the receptor. After a 24-h application, the skin was removed from the Franz cell. The permeant amount within the skin reservoir was extracted by 0.1 N HCl as described previously (12). All samples taken were analyzed by fluorescence spectrophotometer (F2500, Hitachi).

In vivo Percutaneous Absorption

A glass cylinder with a hollow area of 0.785 cm^2 was attached to the porcine back with or without RF by superglue. An aliquot of 0.2 ml of vehicles the same as the *in vitro* experiment was pipetted into the cylinder. The application period was 2 h. The animal was then sacrificed, and the treated skin area was excised. For vertical observation of permeant distribution in the skin, the skin samples were sectioned in a cryostat microtome at a thickness of 20 μm. The slices were monitored with a fluorescence microscope (IX81, Olympus). For the horizontal observation of the skin, a confocal laser scanning microscope (CLSM) was used (TCS SP2, Leica, Wetzlar, Germany). The skin thickness was scanned at 5-μm increments via z-axis. Images were taken by summing 15 fragments at different depths from the skin surface.

Statistical Analysis

Statistical analysis of differences between the groups was carried out using the Kruskal-Wallis test. The post hoc test used for checking individual differences was Dunn's test. A 0.05 level of probability was taken as the level of significance. Statistical measurements were performed with Winks 7.0 version (Texasoft, Duncanville, TX, USA).

RESULTS

In vivo Skin Physiology

Table I summarizes TEWL, skin pH, and erythema of porcine skin with or without bipolar RF treatment at 30 mJ. According to the manufacturer's manual, this energy is described as low impact with minor and superficial ablation on the skin. TEWL increased from 11 to 36 $g/m^2/h$ immediately following RF irradiation. The value obtained for RF was 3 times higher than that obtained from the non-treatment group. No significant difference ($p > 0.05$) between the pH values of the control and the RF-treated groups was detected. Results showed that RF exposure increased a* level from 1.9 to 3.8. However, there was no significance ($p > 0.05$) between the two values due to the large intersubject variation.

Table I The transepidermal water loss (TEWL), pH value, and erythema (a*) of porcine skin treated with or without radiofrequency (RF)

Parameter	No RF	RF at 30 mJ
TEWL ($g/m^2/h$)	11.36 ± 1.05	35.74 ± 6.21
pH value	6.52 ± 0.46	6.43 ± 0.24
a* (arbitrary unit)	1.93 ± 1.11	3.84 ± 1.87

Each value represents the mean ± S.D. ($n = 5$)

Histology of Porcine Skin

The structural changes in RF-treated skin were obtained from macroscopic observation, H&E staining, and TEM. Figure 1a shows the digital photograph of porcine skin after RF application. A faint redness on the skin surface was seen, mainly in the center of the treated zones. Figure 1b exhibits magnified images of the skin surface before and after formation of microchannels. The non-treated skin was intact with some furrows and hairs on the surface. Some micropores on the skin surface treated by RF appeared. The diameter of the microchannels was about 200 μm, simulating the size of the microelectrodes. The size of these pores was very uniform and reproducible. Punch biopsies were taken to be stained with H&E as shown in Fig. 1c. Bipolar RF created the microchannels in the epidermis (arrow in Fig. 1c). The ablation depth reached the bottom of the epidermis. Some SC layers still remained above the microchannels after RF treatment. The size of the micropore was about 170 μm in diameter and 35 μm in depth. The diameter of the pore was consistent with that of RF microelectrodes. The dermis of the control skin showed an irregular parallel arrangement of collagen fibrils. We found an increase of the fibrils. We also found an increase of the fibrils in the superficial dermis under the microchannels. The collagen was located vertically after RF irradiation.

The skin was analyzed by TEM to view ultrastructural change by RF. Figure 1d demonstrates TEM images of the epidermal layers. An intact structure of the epidermis could be seen for the non-treated group. Within an area receiving RF, the intercellular space showed a greater expansion, perhaps caused by spongiosis (arrows in Fig. 1d). This suggests that in addition to the creation of micropores, RF affected the residual tissues. Figure 1e reveals ultrastructural alteration of the upper dermis by RF. The organization of collagen was dense for RF-treated skin. This finding was not observed in the control tissue. The dimension of the fibroblasts in the group of RF was larger than in that of the control group.

Higher Harmonic Generation Microscopy (HGM)

HGM imaging was obtained from the skin surface to the upper dermis. The SC and epidermal morphology can be displayed through the THG signal, while the collagenous structure in the dermis can be revealed by SHG. As shown in Fig. 2a, THG imaging is captured from the skin surface with a 5-μm depth increment (left to right). In the intact skin, the first segment can be categorized as SC. THG contrast was stronger in the SC than in the viable epidermis due to the multilayer structure and intercellular lipids. The optical sections of the deeper layer corresponding to the viable epidermis were characterized by fluorescent cytoplasm surrounding the dark nuclei. However, some bright signal can be observed in the margin of the sample (arrows in Fig. 2a), indicating that some SC was still exist in the depth of >5 μm due to uneven skin surface. The complete SC structure was not observed in the first segment of RF-treated skin. Instead, the first section showed a morphology of viable epidermis with more keratinocytes as compared to non-treatment skin. Similar to the intact skin, the bright region in the margin of RF-treated skin indicated the remnant SC after ablation. Comparison of the length of bright area between intact and RF-treated skin demonstrated a thinner SC layer of skin by RF irradiation (arrows with double heads in Fig. 2a). Moving to the deeper strata, a similar structure to the first segment was seen. Figure 2b shows examples of horizontally sectioned SHG signal at a depth of 50 μm below the skin surface taken from the superficial dermis. The collagen fiber content appeared to be loose, lacking definitive arrangement. RF-treated skin showed a denser and ordered collagen compared to intact skin.

In vitro Percutaneous Absorption

Cutaneous delivery of macromolecules was investigated into and across RF-treated skin *in vitro*. Table II depicts the skin uptake and flux of peptide, siRNAs, and FDs. RF thermolysis resulted in increased skin permeation of peptide. The average skin accumulation of peptide was 3-fold higher than the non-treated skin. Peptide flux after RF management at 30 mJ was 23-times greater than that without RF. siRNA10 and siRNA15 were 6.2- and 2.6-fold more permeable into RF-treated skin compared to the control skin, respectively. The passive flux of both siRNAs was essentially zero. Some siRNA molecules could be found in the receptor after RF exposure. The effect of MW of FDs on skin permeation was determined. The MWs of 10, 20, and 40 kDa were selected owing to the similar sizes of therapeutic macromolecules for biomedical applications. There was no significant difference ($p > 0.05$) among passive skin accumulation of three FDs. RF enhanced skin deposition of FD10 by 3-fold ($p < 0.05$), while this epidermal ablation increased skin uptake of FD20 and FD40 by 4- and 5-fold. RF also delivered 4-fold more FD10 into the receptor than the non-treated group. The intact skin demonstrated a significant barrier to FD20 and FD40, with undetectable

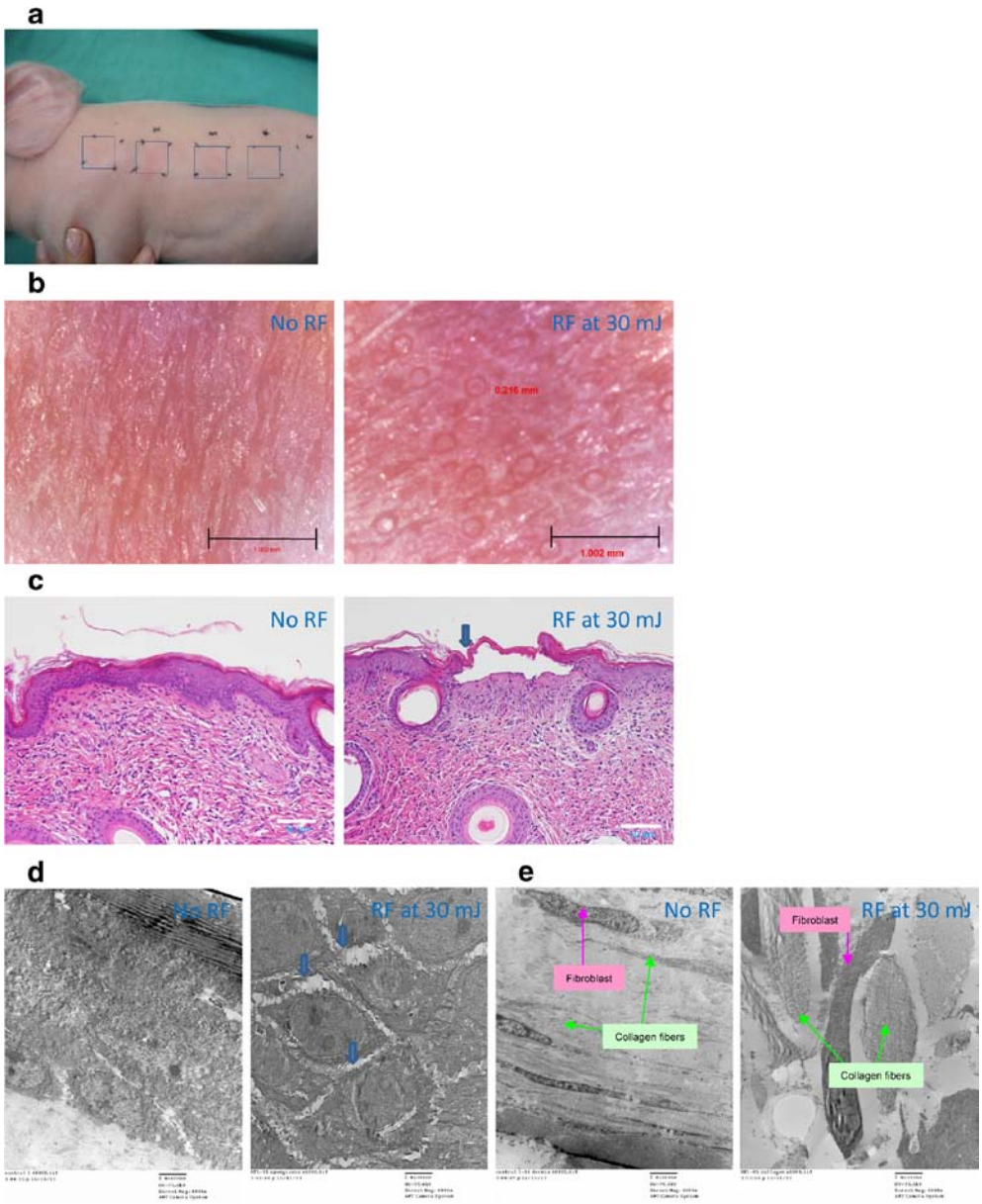

Fig. 1 The porcine skin structure treated with and without radiofrequency (RF): (**a**) Digital photograph of porcine skin surface after RF application. The square is the treatment zone. (**b**) The magnified images of skin surface with and without RF treatment. (**c**) The H&E-staining histology of skin with and without RF treatment. (**d**) TEM images of epidermis with and without RF treatment. (**e**) TEM images of upper dermis with and without RF treatment.

penetration into the receptor. Following thermolysis, the respective flux of FD20 and FD40 could be increased to 0.14 and 0.22 nmol/cm^2/h. These results suggest that RF could deliver macromolecules into and across the skin by breaching the permeation barrier.

In addition to the energy of 30 mJ, the skin accumulation of macromolecules was also studied by a lower strength of 20 mJ. As shown in Fig. 3, by changing the energy from 30 to 20 mJ, the skin uptake of macromoles was generally decreased slightly. There was no significant difference (p >0.05) of skin accumulation between the different energies for siRNAs and FD with lower MWs (FD10 and FD20). On the other hand, the increase of the ablation force led to an increase of peptide and FD40 accumulation (p <0.05) although this increase was less than 2-fold.

In vivo Percutaneous Absorption

In vivo skin absorption of peptide and siRNA15 was examined by fluorescence microscopy at 2 h post-application of RF. The left panel of Fig. 4 is the merging of H&E histology and fluorescence images. The real fluorescence micrographs are shown in the right panel. As illustrated in Fig. 4a, the fluorescence expression of peptide in intact skin is confined to the superficial layers and hair follicles. The skin section treated with RF reveals an intense fluorescence from the skin surface to the lower dermis. H&E histology showed some micropores (arrows in Fig. 4a) in the epidermis perforated by RF. The peptide appeared to diffuse to the peripheral regions of the pores, resulting in a homogeneous distribution of fluorescence in whole skin. A similar result was observed in the skin

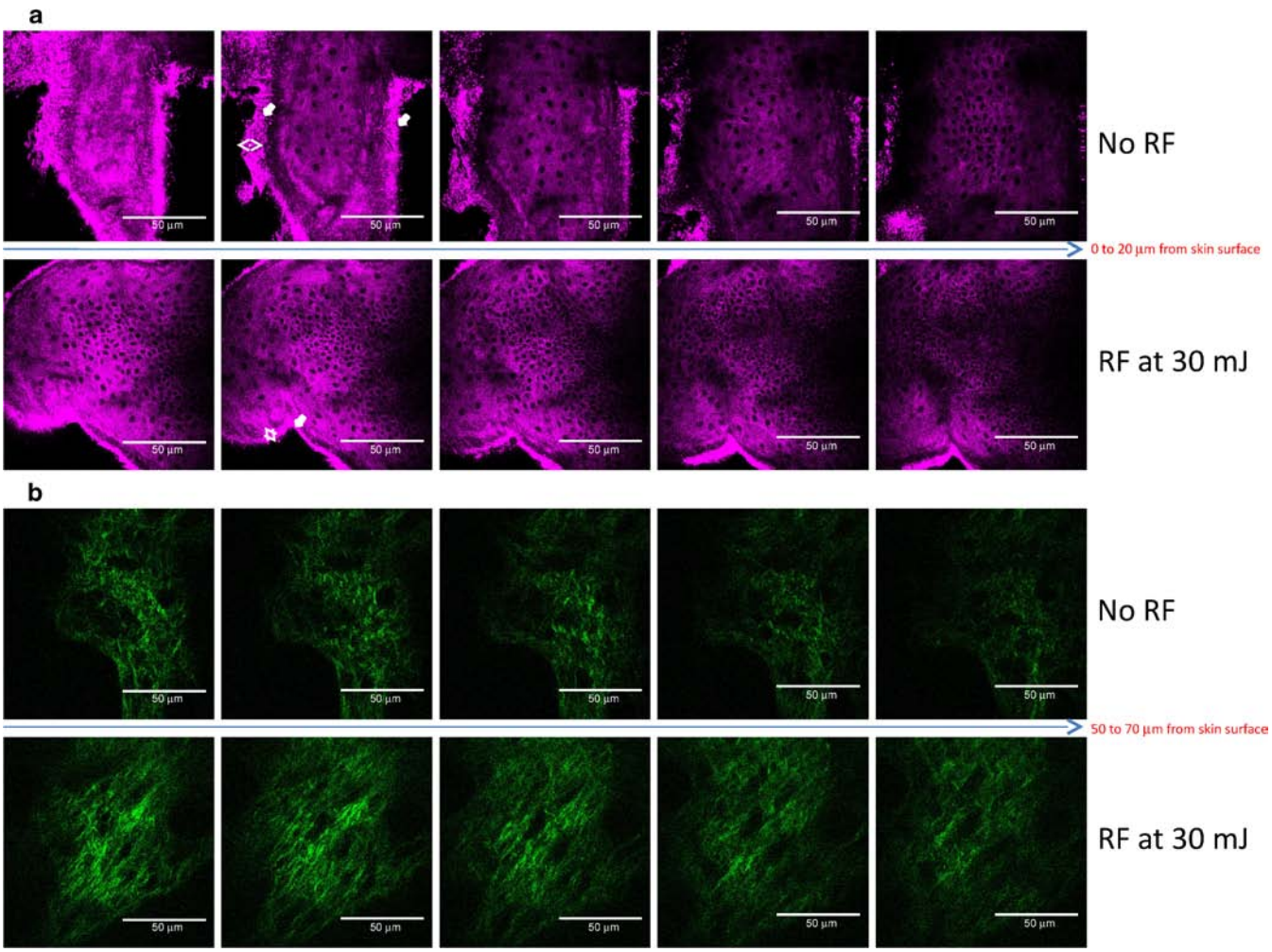

Fig. 2 The porcine skin treated with and without radiofrequency (RF) examined by higher harmonic generation microscopy (HGM): (**a**) Third harmonic generation (THG) contrast of skin with and without RF (skin depth of 0 to 20 μm). (**b**) Second harmonic generation (SHG) contrast of skin with and without RF (skin depth of 50 to 70 μm).

absorption of siRNA15 (Fig. 4b). After administration of siRNA15 to the ablated skin, the viable skin and follicles were stained by fluorescence. The fluorescence was not limited to the specific site of the microchannels, but was also visible in the entire treated region.

The CLSM profiles are shown in Fig. 5. We acquired the *x-y* planed sectional imaging from the skin surface with a 5-μm increment. The right panel exhibited the summary of 15 fragments. The results demonstrated that RF application could enhance fluorescence intensity of peptide and siRNA distributed in the skin (Fig. 5a and b). The most intense signal was seen inside the micropores (arrows) and the sites lateral to the ablated areas. The diameter of the fluorescence-stained pores was 200 ~ 250 μm, indicating a radial distribution of the permeants. The intense fluorescence of the peptide could reach a depth of at least 74 μm after RF exposure. siRNA15

Table II The *in vitro* skin accumulation (*nmol/g*) and flux ($\mu g/cm^2/h$) of peptide, siRNA10, siRNA15, FD10, FD20, and FD40 via porcine skin treated with or without radiofrequency (RF)

Permeant	Skin accumulation (nmol/g)		Flux (nmol/cm^2/h)	
	No RF	RF at 30 mJ	No RF	RF at 30 mJ
Peptide	7.15 ± 3.19	21.23 ± 1.79	0.05 ± 0.02	1.13 ± 0.05
siRNA10	0.29 ± 0.09	1.79 ± 0.43	0	0.03 ± 0.003
siRNA15	0.60 ± 0.31	1.55 ± 0.73	0	0.09 ± 0.01
FD10	0.19 ± 0.01	0.61 ± 0.23	0.42 ± 0.03	1.31 ± 0.22
FD20	0.20 ± 0.07	0.85 ± 0.14	0	0.14 ± 0.02
FD40	0.13 ± 0.06	0.62 ± 0.15	0	0.22 ± 0.05

Each value represents the mean ± S.D. ($n = 4$)

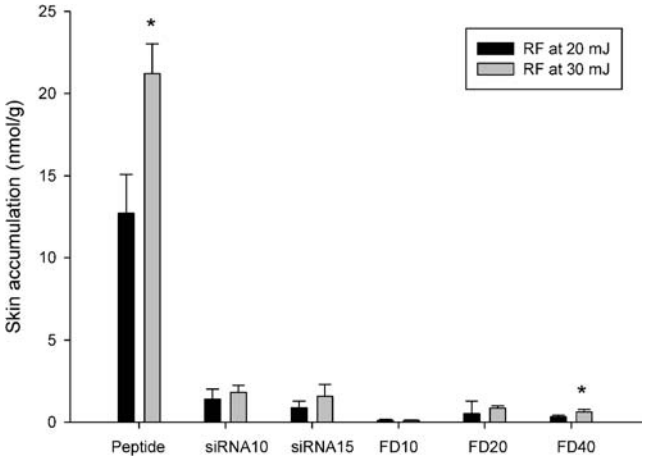

Fig. 3 A comparison of *in vitro* skin accumulation (*nmol/g*) of macromolecules after radiofrequency (RF) treatment at 20 and 30 mJ. Each value represents the mean ± S.D. ($n = 4$).

reached a shallower layer of about 50 μm as compared to the peptide. This may have been due to the higher MW of siRNA.

DISCUSSION

Improved and minimally invasive delivery methods are necessary for topical macromolecule administration. Removal of SC or superficial skin by tape-stripping, chemical treatment, and mechanical abrasion has been demonstrated to enhance macromolecule delivery. Nevertheless, these strategies are limited for application due to insufficient control and reproducibility, and also because they cause significant skin damage (13). In the present work, we utilized fractional RF for promoting delivery of macromolecules into the skin with the reservoir of the skin's barrier function. Some erythema could be found according to colorimetry and macroscopic observation. The heating effect resulted in vasodilation and acute inflammation (14). Although skin redness was observed, we found that this phenomenon could be diminished 2 h post-treatment.

The conduction of heat contributed to the production of microchannels. Some remnants of SC layers still existed above the micropores, indicating an ability of selective ablation by RF array. This phenomenon was also observed by fractional CO_2 laser resurfacing (15, 16). The RF type and energy applied can be configured to target specific tissues (17). The fractional RF at 30 mJ generated tissue ablation deep below the SC. The predominant ablation area was at the epidermis. This effect has been termed "sublative" or "micro-ablative" treatment (18, 19). The RF approach investigated herein induced selective resurfacing to the epidermis with minimal damage to the surrounding tissues. The remnant SC assured the integrity of the skin barrier for the body's defense. TEWL is an indicator of the SC barrier function. A previous study (20) demonstrates an increase of TEWL from 14 to 68 g/m^2/

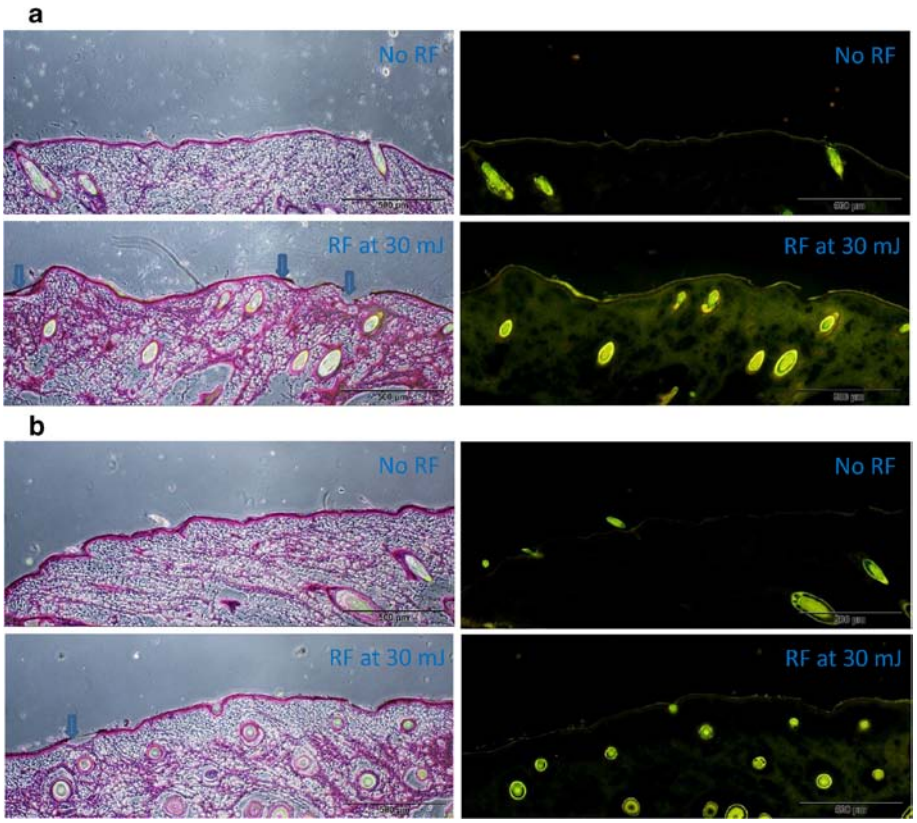

Fig. 4 Fluorescence microscopic images of porcine skin treated with and without radiofrequency (RF): (**a**) Topical peptide application for 2 h. (**b**) Topical siRNA15 application for 2 h. The left panel is the superimposed picture of the fluorescence and H&E-stained images; the right panel is the fluorescence image detected at 450～490 and 515～565 nm for excitation and emission.

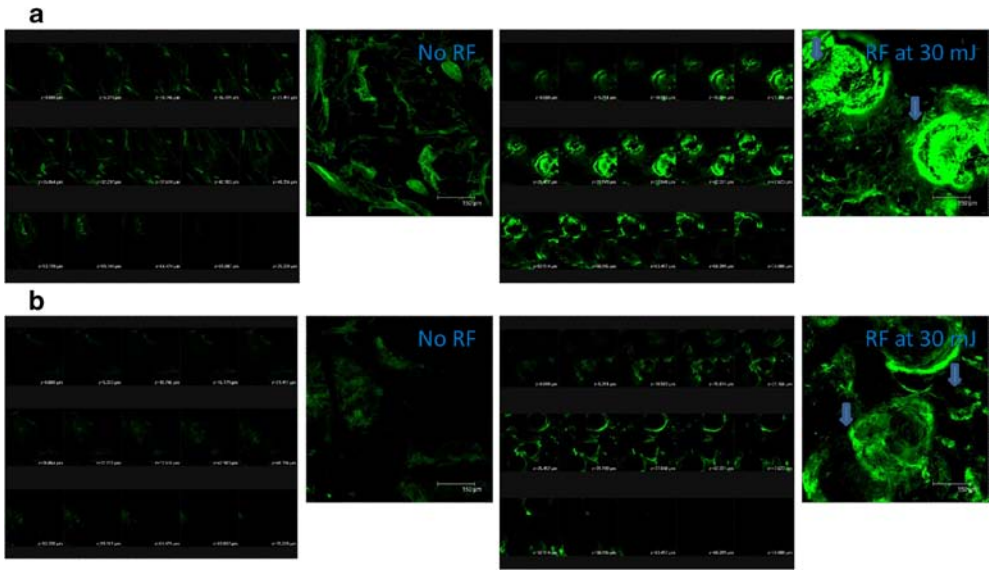

Fig. 5 Confocal micrographs of porcine skin treated with and without radiofrequency (RF): (**a**) Topical peptide application for 2 h (skin depth of 0 to 75 μm). (**b**) Topical siRNA15 application for 2 h (skin depth of 0 to 75 μm). The right panel is a summary of 15 fragments at various skin depths.

h after fractional skin ablation by microneedles. Another report (21) utilizing rat skin as the barrier shows a 10~25-fold increase of TEWL after microneedle puncture. We showed a 3-fold TEWL increase by RF at 30 mJ, which was significantly less than that induced by microneedles. This confirmed the superior safety of bipolar RF technique.

RF used for rejuvenation may cause side effects such as skin burning, scaring, and atrophy (22). Most adverse effects result from inadequate energy setting. The energy used in this work (20 and 30 mJ) was lower than that used for rejuvenation. A quick re-epithelialization and regrowth of new tissues into the microchannels was expected due to the migration of normal tissue/cells to the wounded sites. An example of fast micropore recovery is observed for fractional laser resurfacing (23). Less than 5% of treated surface was occupied by micropores, demonstrating a limited damage to the skin. The skin surface should only be heated at a time scale of microseconds for bypassing significant temperature elevation in viable cells and nerve endings (24). The pulse duration of the fractional RF was within microseconds, indicating that deeper skin strata did not experience a momentous temperature rise. Fractional RF may appear to be well tolerated with the energy restricted to the epidermis; thus dermal nociceptors were not influenced. The pain sensation may be minor since the occurrence of the pain threshold by heat is about 43°C (25).

HGM is a new modality for virtual biopsy at the subcellular scale. With the combination of THG and SHG, it is an ideal tool for analyzing skin morphology (26). Quite different morphologies could be observed between the skin treated with and without sublative RF. A smaller size with an increased density of keratinocytes was shown right at the surface of RF-treated skin. These unique characteristics are the typical feature of the deeper epidermis (27, 28). This result suggests the ablation of the epidermis by RF. According to HGM, the remnant SC after RF irradiation was thinner than the intact SC of non-treated skin. This indicates the partial but not complete ablation of SC by RF. According to SHG imaging, an increase in fibril amounts of collagen was exhibited for RF-treated skin. This trend was well correlated with the clinical findings that collagen dissociation occurs immediately after RF treatment (29, 30). The heat has specific effects on collagen by breaking hydrogen bonds in triple helixes.

Although the therapeutic targets of peptides/proteins and genes to the skin have been identified, translation to clinics is always hindered by insufficient delivery into the skin. Our results suggested a successful way to elicit peptide and siRNA transport via the skin by sublative RF. In order to assure the integrity of macromolecules after penetration into skin, we had performed a preliminary stability test with a size-exclusion column (Sephadex G-25). The fluorescence in the collected fraction was determined by fluorescence spectrometry. The macromolecules tested (peptide, siRNAs, and FDs) had the same elution profiles for both donor and receptor compartments at the end of *in vitro* permeation experiment, indicating the negligible degradation throughout the experimental period (24 h). The permeation was greater by applying higher RF fluence although this difference was not large. RF-created microchannels residing in the epidermis were governable with efficient skin delivery (31). In addition to the SC, the tight junction in the epidermis plays a principal role as a penetration barrier, especially for macromolecules (16). The nature of microchannels is basically hydrophilic (32). Peptides and siRNAs are regarded as hydrophilic and highly water-soluble (2, 33), showing facile entrance into microchannels. RF-generated microchannels provide an appropriate dimension for topical delivery of macromolecules. As depicted in TEM and HGM, RF not only ablated the epidermis but also disrupted the remaining skin structures. Previous studies (7,

34) provide the evidence that RF produced homogenization of the SC. Thus the macromolecules could easily penetrate into the discomposed skin.

The peptide illustrated higher permeation than siRNAs and FDs owing to lower MW, suggesting the possible role of permeant size on RF-mediated absorption. Another possibility is the strong interaction of peptides to the SC and the epidermis for localization in the skin reservoir (35). It is interested to compare skin penetration of siRNA10 and FD10 that possess similar MW. siRNA10 preferred to be accumulated in the skin reservoir with an inferior penetration into the receptor, whereas FD10 exhibited a contrary tendency. The difference of constituents and conformations between the two permeants may contribute to the different permeation manners. Dextrans are unbranched polyglucans that present a linear conformation (36). siRNA is composed of nucleotides with a folding structure (37). The flux of FDs by thermolysis was generally reduced following the increase of MW. A cutoff limit of MW by RF-assisted delivery was not achieved since cutaneous delivery of FD40 could be enhanced by fractional ablation. This demonstrates that topical penetration of macromolecules of at least 40 kDa can be reached with RF.

In vivo skin permeability can be an order of magnitude greater than *in vitro* permeation (24). Our *in vivo* experiments evaluated by fluorescence and confocal microscopies had suggested a superior delivery of peptide and siRNA15 actuated by RF. Peptide and siRNA15 were heavily accumulated in the follicles. This is reasonable since appendageal routes are essential for macromolecule absorption (38). The imaging also showed that the fluorescence distribution was not only confined at the ablated site, indicating a rapid diffusion of permeants from the microchannels and disrupted skin to the deeper skin strata. In addition to vertical diffusion to the deeper skin layers, the macromolecules radially diffused to the lateral regions. The radial distribution of fluorescence in CLSM profiles confirmed this inference. The increase in the diffusion area with microchannels led to more efficient absorption of the permeants.

Fractional ablation by lasers, microneedles, and RF is employed to assist topical drug delivery. The skin color can influence the effectiveness of laser treatment. Moreover, a bulky and expensive device limits the extensive use of laser treatment. Our previous study (39) had examined the laser-assisted peptide permeation by fractional Er: YAG laser. The experimental results showed a 4-fold enhancement of the peptide (2335 Da) flux by the laser. RF used in the present work displayed an increment of peptide flux by a 23-fold, indicating the applicability of RF as the enhancement approach for macromolecule delivery. The elasticity and irregular surface of the skin are challenges in the reproducibility of microneedle insertion (40). The insertion pressure is always variable by different operators. Bipolar RF was shown to be cost-effective. The ablation depth can be precisely controlled by modulating the fluence. Selective removal of the epidermis without significantly damaging the SC by sublative RF offers an opportunity to develop a safe and efficient strategy for enhancing topical macromolecule delivery. Hruza . (41) have investigated the skin recovery of subjects treated by Matrix® RF, a fractional RF supplied by Syneron, with 3 courses during 3~4 weeks. Complete tissue healing was achieved within 2 days by an ablation to a depth to epidermis. The epidermis had completely re-epithialized 24 h post-operation. Minimal erythema and skin irritation could be observed in this duration. This may indicate the tolerance of this device for long-term use. Further study is needed to fully explore the safety issue and the recovery for RF-exposed skin. siRNA15 is an active used for treating pachyonychia congenital by intradermal injection (42), which is a disease with a sign of keratoderma. RF-mediated administration may avoid the intradermal administration of siRNA to the nidus. The induction of the silencing effect by topically applied siRNA only shows a successful rate of <50% (33). RF approach may increase the successful rate because of its ability to enhance siRNA delivery.

CONCLUSIONS

The findings of this work represent the first report on RF-assisted topical delivery of peptide and siRNA. The fractional RF provided advantages for less-invasive heating of selective tissues. As shown in this study, the electrical field generated by RF resulted in greater removal of the epidermis than of the SC and dermis. The enhancement of skin absorption through the microchannels and the penetration depth was dependent upon the molecular size and steric structure of the permeants. Besides the creation of microchannels, structural disruption of residual tissues was another mechanism inducing permeation enhancement. This tendency has been adapted as an optional approach for peptide and gene delivery. Given these encouraging results, the future perspective is to examine the feasibility of RF-assisted macromolecule transport in humans.

REFERENCES

1. Peer D, Lieberman J. Special delivery: targeted therapy with small RNAs. Gene Ther. 2011;18:1127–33.
2. Benson HAE, Namjoshi S. Proteins and peptides: strategies for delivery to and across the skin. J Pharm Sci. 2008;97:3591–610.
3. Lee WR, Pan TL, Wang PW, Zhuo RZ, Huang CM, Fang JY. Erbium:YAG laser enhances transdermal peptide delivery and skin vaccination. J Control Release. 2008;128:200–8.
4. Desai PR, Marepally S, Patel AR, Voshavar C, Chaudhuri A, Singh M. Topical delivery of anti-TNFα siRNA and capsaicin via novel lipid-polymer hybrid nanoparticles efficiently inhibits skin inflammation in vivo. J Control Release. 2013;170:51–63.

5. Alexiades-Armenakas MR, Dover JS, Arndt KA. The spectrum of laser skin resurfacing: nonablative, fractional, and ablative laser resurfacing. J Am Acad Dermatol. 2008;58:719–37.
6. Goldberg DJ, Berlin AL, Phelps R. Histologic and ultrastructural analysis of melasma after fractional resurfacing. Lasers Surg Med. 2008;40:134–8.
7. Alvarez N, Ortiz L, Vicente V, Alcaraz M, Sánchez-Pedreño P. The effects of radiofrequency on skin: experimental study. Lasers Surg Med. 2008;40:76–82.
8. Chandrasekhar S, Iyer LK, Panchal JP, Topp EM, Cannon JB, Ranade VV. Microarrays and microneedle arrays for delivery of peptides, proteins, vaccines and other applications. Expert Opin Drug Deliv. 2013;10:1155–70.
9. Lin CH, Aljuffali IA, Fang JY. Lasers as an approach for promoting drug delivery via skin. Expert Opin Drug Deliv. 2014;11:599–614.
10. Pan TL, Wang PW, Lee WR, Fang CL, Chen CC, Huang CM, *et al.* Systematic evaluations of skin damage irradiated by an erbium:YAG laser: histopathologic analysis, proteomic profiles, and cellular response. J Dermatol Sci. 2010;58:8–18.
11. Lee JH, Tsai MR, Sun CK, Chiang BL. Evaluation of the role of CD207 on Langerhans cells in a murine model of atopic dermatitis by *in situ* imaging using Cr:forsterite laser-based multimodality nonlinear microscopy. J Biomed Opt. 2012;17:116007.
12. Hsieh PW, Chen WY, Aljuffali IA, Chen CC, Fang JY. Co-drug strategy for promoting skin targeting and minimizing transdermal diffusion of hydroquinone and tranexamic acid. Curr Med Chem. 2013;20:4080–92.
13. Lee WR, Shen SC, Liu CJ, Fang CL, Hu CH, Fang JY. Erbium:YAG laser-mediated oligonucleotide and DNA delivery via the skin: an animal study. J Control Release. 2006;115:344–53.
14. Choi S, Cheong Y, Shin JH, Lee HJ, Lee GJ, Choi SK, *et al.* Short-term nanostructural effects of high radiofrequency treatment on the skin tissues of rabbits. Lasers Med Sci. 2012;27:923–33.
15. Haak CS, Illes M, Paasch U, H dersdal M. Histological evaluation of vertical laser channels from ablative fractional resurfacing: an ex vivo pig skin model. Lasers Med Sci. 2011;26:465–71.
16. Lee WR, Shen SC, Aljuffali IA, Li YC, Fang JY. Impact of different vehicles for laser-assisted drug permeation via skin: full-surface versus fractional ablation. Pharm Res. 2014;31:382–93.
17. Wollina U. Treatment of facial skin laxity by a new monopolar radiofrequency device. J Cutan Aesthet Surg. 2011;4:7–11.
18. Elman M, Harth Y. Novel multi-source phase-controlled radiofrequency technology for non-ablative and micro-ablative treatment of wrinkles, lax skin and acne scars. Laser Ther. 2011;20:139–44.
19. Lee HS, Lee DH, Won CH, Chang HW, Kwon HH, Kim KH, *et al.* Fractional rejuvenation using a novel bipolar radiofrequency system in Asian skin. Dermatol Surg. 2011;37:1611–9.
20. Gomaa YA, Morrow DIJ, Garland MJ, Donnelly RF, El-Khordagui LK, Meidan VM. Effects of microneedle length, density, insertion time and multiple applications on human skin barrier function: assessments by transepidermal water loss. Toxicol in vitro. 2010;24:1971–8.
21. Yan G, Warner KS, Zhang J, Sharma S, Gale BK. Evaluation needle length and density of microneedle arrays in the pretreatment of skin for transdermal drug delivery. Int J Pharm. 2010;391:7–12.
22. Sadick S. Bipolar radiofrequency for facial rejuvenation. Facial Plast Clin N Am. 2007;15:161–7.
23. Chen X, Shah D, Kositratna G, Manstein D, Anderson RR, Wu MX. Facilitation of transcutaneous drug delivery and vaccine immunization by a safe laser technology. J Control Release. 2012;159:43–51.
24. Lee JW, Gadiraju P, Park JH, Allen MG, Prausnitz MR. Microsecond thermal ablation of skin for transdermal drug delivery. J Control Release. 2011;154:58–68.
25. Franco W, Kothare A, Ronan SJ, Grekin RC, McCalmont TH. Hyperthermic injury to adipocyte cells by selective heating of subcutaneous fat with a novel radiofrequency device: feasibility studies. Lasers Surg Med. 2010;42:361–70.
26. Tsai MR, Lin CY, Liao YH, Sun CK. Applying tattoo dye as a third-harmonic generation contrast agent for in vivo optical virtual biopsy of human skin. J Biomed Opt. 2013;18:026012.
27. Tsai TH, Jee SH, Chan JY, Lee JN, Lee WR, Dong CY. Visualizing laser-skin interaction in vivo by multiphoton microscopy. J Biomed Opt. 2009;14:024034.
28. Koehler MJ, Speicher M, Lange-Asschenfeldt S, Stockfleth E, Metz S, Elsner P, *et al.* Clinical application of multiphoton tomography in combination with confocal laser scanning microscopy for in vivo evaluation of skin diseases. Exp Dermatol. 2011;20:589–94.
29. Seidenari S, Arginelli F, Bassoli S, Cautela J, French PM, Guanti M, *et al.* Multiphoton laser microscopy and fluorescence lifetime imaging for the evaluation of the skin. Dermatol Res Prac. 2012;2012:810749.
30. Edward AF, Massaki ABMN, Fabi S, Goldman M. Clinical efficacy and safety evaluation of a monopolar radiofrequency device with a new vibration handpiece for the treatment of facial skin laxity: a 10-month experience with 64 patients. Dermatol Surg. 2013;39:104–10.
31. Birchall J, Coulman S, Anstey A, Gateley C, Sweetland H, Gershonowitz A, *et al.* Cutaneous gene expression of plasmid DNA in excised human skin following delivery via microchannels created by radio frequency ablation. Int J Pharm. 2006;312:15–23.
32. Levin G, Gershonowitz A, Sacks H, Stern M, Sherman A, Rudaev S, *et al.* Transdermal delivery of human growth hormone through RF-microchannels. Pharm Res. 2005;22:550–5.
33. Chong RHE, Gonzalez-Gonzalez E, Lara MF, Speaker TJ, Contag CH, Kaspar RL, *et al.* Gene silencing following siRNA delivery to skin via coated steel microneedles: in vitro and in vivo proof-of-concept. J Control Release. 2013;166:211–9.
34. Tsai TH, Lin SJ, Lee WR, Wang CC, Hsu CT, Chu T, *et al.* Visualizing radiofrequency-skin interaction using multiphoton microscopy in vivo. J Dermatol Sci. 2012;65:95–101.
35. Lanke SSS, Kolli CS, Strom JG, Banga AK. Enhanced transdermal delivey of low molecular weight heparin by barrier perturbation. Int J Pharm. 2009;365:26–33.
36. Fang JY, Lee WR, Shen SC, Wang HY, Fang CL, Hu CH. Transdermal delivery of macromolecules by erbium:YAG laser. J Control Release. 2004;100:75–85.
37. Lu ZJ, Mathews DH. Efficient siRNA selection using hybridization thermodynamics. Nucleic Acids Res. 2008;36:640–7.
38. Wosicka H, Cal K. Targeting to the hair follicles: current status and potential. J Dermatol Sci. 2010;57:83–9.
39. Lee WR, Shen SC, Al-Suwayeh SA, Yang HH, Yuan CY, Fang JY. Laser-assisted topical drug delivery by using a low-fluence fractional laser: imiquimod and macromolecules. J Control Release. 2011;153:240–8.
40. Kim J, Jang JH, Lee JH, Choi JK, Park WR, Bae IH, *et al.* Enhanced topical delivery of small hydrophilic or lipophilic active agents and epidermal growth factor by fractional radiofrequency microporation. Pharm Res. 2012;29:2017–29.
41. Hruza G, Taub AF, Collier SL, Mulholland SR. Skin rejuvenation and wrinkle reduction using a fractional radiofrequency system. J Drug Dermatol. 2009;8:259–65.
42. Smith FJD, Hickerson RP, Sayers JM, Reeves RE, Contag CH, Leake D, *et al.* Development of therapeutic siRNAs for pachyonychia congenital. J Investig Dermatol. 2008;128:50–8.